

Enhanced Correction Methods for High Density Hot Pixel Defects in Digital Imagers

Glenn H. Chapman^{*a}, Rahul Thomas^a, Rohit Thomas^a, Zahava Koren^b, Israel Koren^b

^aSchool of Engineering Science, Simon Fraser University, Burnaby, BC, Canada, V5A 1S6

^bDept. of Electrical & Computer Engineering, Univ. of Massachusetts, Amherst, MA, USA 01003

ABSTRACT

Our previous research has found that the main defects in digital cameras are “Hot Pixels” which increase at a nearly constant temporal rate. Defect rates have been shown to grow as a power law of the pixel size and ISO, potentially causing hundreds to thousands of defects per year in cameras with <2 micron pixels, thus making image correction crucial. This paper discusses a novel correction method that uses a weighted combination of two terms - traditional interpolation and hot pixel parameters correction. The weights are based on defect severity, ISO, exposure time and complexity of the image. For the hot pixel parameters component, we have studied the behavior of hot pixels under illumination and have created a new correction model that takes this behavior into account. We show that for an image with a slowly changing background, the classic interpolation performs well. However, for more complex scenes, the correction improves when a weighted combination of both components is used. To test our algorithm’s accuracy, we devised a novel laboratory experimental method for extracting the true value of the pixel that currently experiences a hot pixel defect. This method involves a simple translation of the imager based on the pixel size and other optical distances.

Keywords: imager defect detection, hot pixel development, active pixel sensor APS, CCD, APS/CCD defects rates, imager defect correction

1. INTRODUCTION

The field of digital imaging and its associated technology has become a central focus of study and research in today’s world of photography. Digital imagers have spread into everyday products ranging from cell phones to embedded sensors in cars. They play a vital role in medical, industrial and scientific applications and are increasing in many engineering solutions. The inherent result is a drive to enhance these sensors via a decrease in pixel size and an increase in the sensitivity of the imager. Given that digital imager sensors are microelectronic in nature, they are susceptible to developing defects over time. In contrast to other devices, most in-field defects in digital imagers begin appearing soon after fabrication, are permanent, and their number increases continuously over the lifetime of the sensor. These permanent defects pose a serious problem for various applications where image quality and pixel sensitivity are a priority.

Our research for the past several years had mainly focused on the development of in-field defects, their characterization and growth rate [1-6]. These studies have resulted in an empirical formula, which projects that as the pixel size shrinks and the sensitivity increases, defect numbers will grow via a power law of the inverse of the pixel size to the 3.3. It also suggests that as pixel sizes decrease to lower than two microns, and sensitivities move towards allowing low light night pictures, defect rates can grow to hundreds or even thousands per year. The defect growth rate is modeled as a function of pixel size, sensor area and ISO. It is our belief that in-field defects are likely the result of cosmic ray damage [1-3].

* glennc@cs.sfu.ca; phone: 1-778-782-3814; fax 1-778-782-4951; <http://www.ensc.sfu.ca/people/faculty/chapman/>;
School of Engineering Science, Simon Fraser University, 8888 University Drive, Burnaby, BC V5A 1S6, Canada

This type of damage cannot be prevented by shielding, which further emphasizes the importance of characterizing these defects and creating algorithms to correct them in-field.

The most common method for defect correction in the field without lab calibration is the classic nearest neighbors' interpolation. This method is based on simple averaging of the faulty pixel's neighbors and may not yield ideal results due to the large number of corrections, and as one or more of the neighbors could also be faulty. Furthermore, interpolation breaks down in busy scenes where there are larger contrasts between neighboring pixels. We suggest a novel correction algorithm which considers the local busyness of the pixels, and based on predefined weights uses a combination of interpolation with hot pixel correction methods. We then experimentally compare the correction results of our algorithm to those of conventional interpolation methods. Even with this ability to correct hot pixel defects with greater accuracy by knowing the pixel defect parameters, we are still left with some amount of error in our correction.

In order to assess the effectiveness of our correction algorithm we need to compare the corrected value to the 'true' pixel value. Complicated methods were employed in the past to extract these true pixel values which in turn proved to be ineffective. In this paper, we use a simpler but accurate method to extract the true value of the defective pixel, by moving the camera. This procedure can, unfortunately, be performed only in lab conditions, but we found it useful to assess the accuracy of our different correction algorithms. One key point to note is that our methods do not involve injecting errors in known locations to assess the effectiveness of our algorithms. Rather, we make use of real photographs with a range of complexities as test images, allowing a more precise evaluation of the quality of our correction algorithm.

One key element in our algorithm is the hot pixel correction method that relies heavily on the knowledge and characterization of hot pixels. This further justifies the study of hot pixels and their nature. Recent research had uncovered that hot pixel's behavior is very sensitive to light. In this paper we briefly explore the effects of illumination on hot pixel behavior and compare our experimental results to the classic hot pixel model.

This paper is organized as follows: **Section 2** presents the classic model of hot pixels. **Section 3** describes the growth rate of the hot pixels. **Section 4** presents the algorithm we propose for correcting these defective pixels. **Section 5** describes the numerical experiments we conducted to validate the effectiveness of our algorithm, and **Section 6** discusses possible correction limitations. **Section 7** explores the effects of illumination on hot pixel behavior, and **Section 8** concludes the paper.

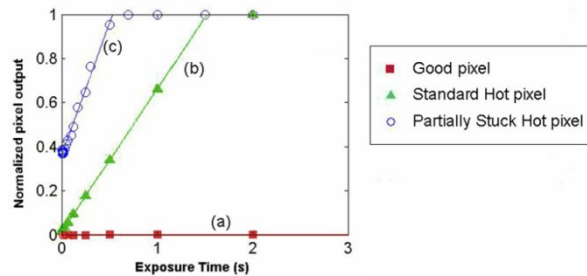


Figure 1: Comparing the dark response of a good pixel and a hot pixel.

2. CLASSIC MODEL OF HOT PIXELS

Over the past 10 years [5,6], we have been studying the characteristics of imager defects by manually calibrating many commercial cameras, including 24 Digital Single Lens Reflex (DSLRs), using dark field exposure (i.e., no illumination). This allowed us to identify stuck-high and partially stuck defects; however, up until now we have not identified any stuck pixel types in our experiments, only hot pixels. The standard hot pixel has a dark response that has an illumination-independent component that increases linearly with exposure time. These types of hot pixels can be identified by capturing a series of dark field images at increasing exposure times. Figure 1 displays the dark response of a hot pixel, showing the normalized pixel illumination vs. the exposure time where illumination level 0 represents no illumination and level 1 represents saturation. Three different pixel responses are shown in Figure 1. Curve (a) shows

the response of a good pixel. Since there is no illumination, we expect the pixel output to be constantly zero for all exposures. The other two curves depict the two different types of hot pixels [5]. Curve (b) is the response of a standard hot pixel which has an illumination-independent component that increases linearly with exposure time. The third response, see curve (c), is a partially stuck hot pixel which has an additional offset that manifests itself at no exposure. Although the overall digital imager is generally considered a digital device, the sensor itself is analog in nature. The classic assumed response of good and hot pixels to illumination can be modeled using Equation (1), where I_{pixel} is the response, R_{photo} measures the incident illumination rate, R_{dark} is the dark current rate, T_{exp} is the exposure time, b is the dark offset, and m is the amplification from the ISO setting.

$$I_{pixel}(R_{photo}, R_{dark}, T_{exp}, b) = m * (R_{photo}T_{exp} + R_{dark}T_{exp} + b) \quad (1)$$

For a good pixel, both R_{dark} and b are zero, and the output is therefore solely dependent on the incident illumination. For a hot pixel, these two terms create a signal that is added to the incident illumination, and therefore the output from such a pixel will appear brighter. The dark response of a pixel, denoted by I_{offset} , can be found by setting R_{photo} to zero which yields:

$$I_{offset}(R_{dark}, T_{exp}, b) = m * (R_{dark}T_{exp} + b) \quad (2)$$

The expression for the dark response (also called the combined dark offset) is linear. Therefore, the parameters R_{dark} and b can be extracted by fitting the pixel response in a dark frame vs. exposure time, as seen in Figure 1. For standard hot pixels, b is zero. These types of hot pixels are generally visible at larger exposure times, while the partially stuck generally appear in all images as the magnitude of b affects the response. Obtaining this data for each camera involves typically 5 to 20 calibration images per test at a wide range of exposure times and ISO's, and their analysis with specialized software [2-4].

Using 24 DSLR camera including both APS and CCD sensors ranging from 1 and 10 years in age [9], we have been able to identify hot pixels. We have detected 243 hot pixels of which 44% were of the partially stuck type at ISO 400. Partially stuck hot pixels have a greater impact on images than standard hot pixels as they are evident at lower exposures. The ISO setting in an imager controls the amplification or sensitivity of the pixel output. Higher ISO settings enable objects to be captured under low light conditions or with very short exposures. Therefore, this removes the need for flash or a long exposure time when doing natural light photography. About 12 years ago, most DSLRs had ISO capabilities of 100 – 1600. As sensor technology improved and better noise reduction algorithms were developed, noise levels have been reduced and the usable ISO range has increased considerably, with recent DSLRs having an ISO range of 50 to 12,300 and high-end cameras having a range from 25,600 to 409,600 ISO.

The large number of offset type hot pixels indicates that the development of stuck high pixels in the field may actually be due to the presence of hot pixels with very high offsets. This is consistent with our claim that a stuck hot pixel has not yet been detected.

3. DEFECT GROWTH RATE

Our research has studied the defect growth rate of pixels for various imagers. We have shown that these defects occur randomly over the sensor[1-6] which further indicates that the source of defects is most likely random in nature, such as cosmic rays. These results have also been observed by other authors, who have shown that neutrons seem to create the same hot pixel defect types [7,8]. Our more recent research [9] has developed an empirical formula that characterizes hot pixel growth. The formula is used to relate the defect density D (defects per year per mm² of sensor area) to the pixel size S (in microns) and sensor gain (ISO) via the following equations:

For CCD sensors

$$D = 10^{-1.849} S^{-2.25} ISO^{0.687} \quad (3)$$

and for APS sensors

$$D = 10^{-1.13} S^{-3.05} ISO^{0.505} \quad (4)$$

These equations show that the defect rate increases drastically when the pixel size falls below 2 microns, and is projected to reach 12.5 defects/year/mm² at ISO 25,600 (already available on some high-end cameras). Given that the current trend is to reduce the size of pixels, our experimental results project that the number of these defects will increase to very high levels, which makes the correction of these defects crucial.

4. MODEL AND ALGORITHM FOR DEFECT CORRECTION

The most common way to model a digital imager is as an array of $U \times V$ pixels, with x_{ij} denoting the incident illumination at location (i,j) for a given image. Each x_{ij} consists of separate pixel values, each pertaining to a different color component. The Bayer Color Filter Array (CFA) [3] (red, blue and two greens – see Figure 2a) is predominantly used in digital color imagers. For the purpose of this analysis we will define a repeated CFA pattern as a single CFA pixel. When the camera data is extracted, the individual colors form a single pixel, four of which make up this CFA pixel.



Figure 2: a) Bayer Color Filter Array with k numbering; b) Pixel color array showing surrounding pixels with relative (i,j) .

We denote by $x_{ij}^{(k)}$ the incident illumination of color k (where $k=1,2,3,4$ – see Figure 2a), additionally it is standardized so that $0 \leq x_{ij}^{(k)} \leq 1$.

We then denote by $y_{ij}^{(k)}$ the (standardized) sensor reading of color k in location (i,j) (where $i=1, \dots, U$ and $j=1, \dots, V$ and $k=1,2,3,4$). For a defect-free CFA pixel, $y_{ij}^{(k)} = x_{ij}^{(k)}$ for all $k = 1, \dots, 4$.

Since the hot pixel defects are very small, at most one of the color components per CFA pixel will be hot, and for this k

$$y_{ij}^{(k)} = x_{ij}^{(k)} + a + bT \quad (5)$$

Where $a+bT$ is the offset of the hot pixel defect.

For simplicity of notation, we have removed the indices i, j, k from the discussion in the rest of the paper. Instead, the hot pixels are numbered $m = 1, \dots, M$. x_m denotes the illumination and y_m denotes the sensor reading of the hot (color) pixel m . The defective pixel in the center with the surrounding neighbor pixels is shown in Figure 2b. Any of the R,G,G,B in the center can be hot.

The following notations are used in our correction algorithm:

$A_m^{(4)}$: Conventional corrected value of hot pixel m based on 4 neighbors, i.e., the average of the four nearest neighbors.

For example, if the color Red at (i,j) is faulty, then this averages the values of R (or $k=1$) for $x_{i-1,j}, x_{i+1,j}, x_{i,j-1}, x_{i,j+1}$

$A_m^{(8)}$: Conventional corrected value of hot pixel m based on 8 neighbors which is the average of the eight nearest neighbors.

Again, for the color Red ($k=1$) example, this averages the Red components of $x_{i-1,j-1}$, $x_{i,j-1}$, $x_{i+1,j-1}$, $x_{i-1,j}$, $x_{i,j}$, $x_{i+1,j}$, $x_{i-1,j+1}$, $x_{i,j+1}$, $x_{i+1,j+1}$

We now denote by D_m a partially-corrected value based on the *dark response* parameters of the hot pixel (recall that these are relatively easy to obtain).

$$D_m = y_m - (a + bT) \quad (6)$$

One key point to note is that the 4 and 8 point interpolations give good results only when the 9 pixels of Figure 2b have a light that changes slowly across the image for the given color, i.e., a tilted plain of that color. However, in reality images can include many localized edges and a high level of busyness. Interpolation fails badly in these situations. Better image correction results can be achieved by using hot pixel correction in such situations. Still, our corrected value D_m (Equation (6)) may not be totally accurate as it is based on curve fitting and only on dark field measurements. We therefore suggest a correction algorithm that uses a weighted combination, denoted by C_m , of A_m and D_m .

Our algorithm differentiates between uniform areas on the image and rapidly changing areas, by comparing the two averages $A_m^{(4)}$ and $A_m^{(8)}$ - if they differ by less than a threshold ε , the area is considered uniform, otherwise it is considered "busy". We allow two different sets of weights, α , $(1 - \alpha)$ and β , $(1 - \beta)$ depending on whether the neighborhood is uniform or busy, respectively.

Weighted Corrected Algorithm:

For a hot – pixel value y_m

$$\text{Select } \varepsilon \geq 0, \quad 0 \leq \alpha \leq 1, \quad 0 \leq \beta \leq 1$$

If $\text{abs}(A_m^{(4)} - A_m^{(8)}) \leq \varepsilon$ (indicating a slowly changing area)

$$\text{replace } y_m \text{ by } C_m = \alpha A_m^{(4)} + (1 - \alpha) D_m \quad (7)$$

Otherwise (indicating sudden changes)

$$\text{replace } y_m \text{ by } C_m = \beta A_m^{(4)} + (1 - \beta) D_m$$

If $y_m \geq 0.99$ (indicating saturation)

$$\text{replace } y_m \text{ by } C_m = A_m^{(4)}$$

The algorithm parameters ε , α , and β need to be determined empirically.

5. EXPERIMENTAL DETERMINATION AND TESTING OF HOT PIXEL CORRECTION

Many researchers have tested their defect correction algorithms by artificially injecting defects into standard pictures. However, our experiments have shown this to be inadequate as it does not reflect the interaction between the hot pixel and the surrounding areas that happens in practice. The problem is that the conventional testing approach assumes that the true value of the undamaged pixel at the hot pixel location is known. Any correction algorithmic method (e.g. interpolation) makes assumptions about how the local area of the picture is changing and cannot provide the true value. This is especially a problem where the local scene area is rapidly changing (e.g., edges of objects with color changes). In this section we present an experimental method that allows us to accurately determine the true value of an undamaged pixel at the hot pixel location and use it to test our proposed correction algorithm in the lab on complex scenes.

A series of images of a busy scene were taken to test our algorithm, similar to ones taken by photographers. We avoided uniform scenes (say a uniform gray wall) as this is not typical and is not a good candidate image to test our algorithm. In such cases interpolation would prove to be very effective, giving nearly perfect results. For this test we also require a camera that contains a large number of hot pixels with varying strengths at a single ISO.

Our experiments made use of two DSLRs which we have tested for the last 6 years. The older is approximately 11 years old, while the other is 6 years old. We have found that both cameras yield similar results. The remainder of this paper will describe results for the newer camera only as it has 52 hot pixels of varying strengths at the ISO 800 level.

As a test image, we took a picture of a wall of books, so that the scene changes in many places, but all objects are at about the same distance from the camera (Figure 3a). This image has areas that are slowly changing, good for the interpolation methods, and other areas that are rapidly changing (edges), where the correction D_m is expected to perform better.

The exposure for this scene was carefully selected such that no picture areas were saturated (i.e., no pixel was at the maximum value where it no longer responds to changes in illumination or to the effect of the hot pixel).

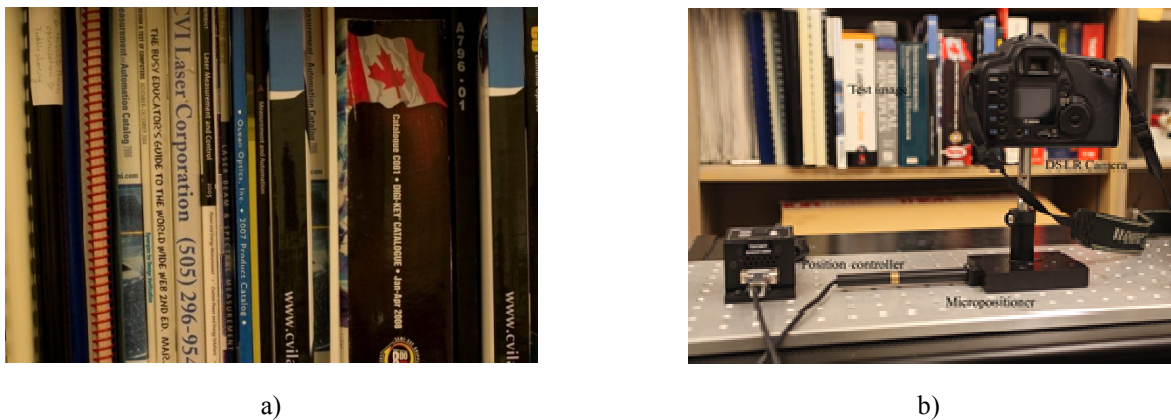


Figure 3: a) Test image for pixel correction; b) Micropositioner for camera motion.

The main challenge in our previous experiments was that we needed the ‘true’ value of the pixel to compare to the corrected value. This true value refers to the pixel minus the defect’s contribution. Previous papers [10] have shown that this is not easily found through analytic methods. Our previous method required us to take the same image with a short exposure, keeping each pixel’s collected light (RT) constant in order to prevent pixels from going into saturation. Additionally, we had to perform curve fitting of the hot pixel response for various exposures under the same amount of illumination using a uniform illuminated image. Such curve fitting allows us to remove the hot pixel effect on the short exposure image of Figure 3a, eventually yielding the real value at the exact location of the defective pixel. Though this method worked, there was no definite way to quantify the error of the obtained value. We have now developed a more reliable and more accurate method to test our correction algorithm.



Figure 4: Depiction of Image Movement Method.

In order to obtain the real value of the defective pixel, the camera is translated to the left (or right) such that the previous image location with the defective pixel is now uncovered. This process makes use of a piezoelectric micro positioner (Figure 3b) to move the camera 128 μm which is twice the pixel width due to the camera lens and the CFA (Figure 3). After this translation, the original location where the defective pixel resided is now relocated to a non-defective pixel of the same corresponding CFA color channel (Figure 4). We are now able to extract the true value for the defective pixel by looking at the moved image two pixels to the right. It is important to note that this method is not needed for the correction; it just helps us compare our correction algorithms by measuring the error due to each of them. One should note that a calibration of the camera with parallel lines is used to determine the needed distance to move the camera 2 pixels. This involves taking an image of the camera with thin parallel lines with large gaps between them. After this, the camera is moved a large distance (about 100-150 pixels) and another image is taken. Using post-processing image programs, we are able to extract the distance needed to move 1 pixel which is then used for the actual test image experiment.

An added benefit of this method is that we essentially obtain two sets of images containing hot pixels from which we can obtain the real value for each defective pixel and test our correction algorithm. The second set is obtained when we use the moved image as the initial position and the initial image before translation as the “moved” image.

The error of this experimental method can be quantified by performing the same extraction method using image locations that do not have defective pixels, and comparing the values before and after the translation of the image. Data was gathered for more than 50 good pixels, resulting in an average error of 6.1% of pixel value with a standard deviation of 6.2%. The shot-to-shot experiment repeatability distribution is shown in Figure 5 for the 1/30 sec exposure (the distribution is very similar for the 1/125 sec exposure). 80% of the errors are <0.004 which is actually below the imager noise floor, so that the error in this method is almost negligible. The noise floor in our sensor is specified as 0.008 by the manufacturer [11], which lines up with our findings.

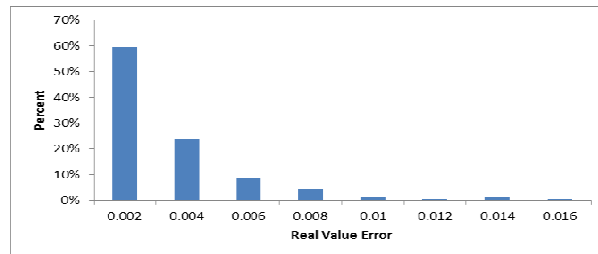
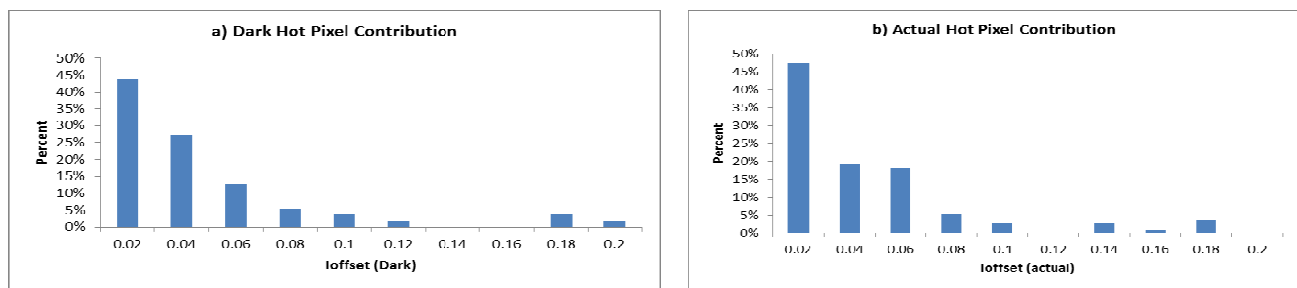


Figure 5: Shot-to-Shot experiment repeatability for 1/30 sec exposure.



a)

b)

Figure 6: Hot pixel contribution for 1/30 sec exposure (a) calculated from dark hot parameters; (b) actual measured hot pixel contribution.

Our experiments show that the hot pixel contribution is initially made up mostly of the dark hot response offset. In Figures 8 and 9 we can see the distribution of the actual hot pixel contribution and the distribution of the dark hot pixel contribution for the 1/30th and 1/125th exposures. It is important to note that even though RT is 0.5 for the 1/30th

exposure compared to the 1/125th exposure, the R for 1/125 sec is 8 times the R for 1/30 sec due to the way we performed the experiments. For this reason we use the dark pixel response value in our correction algorithm.

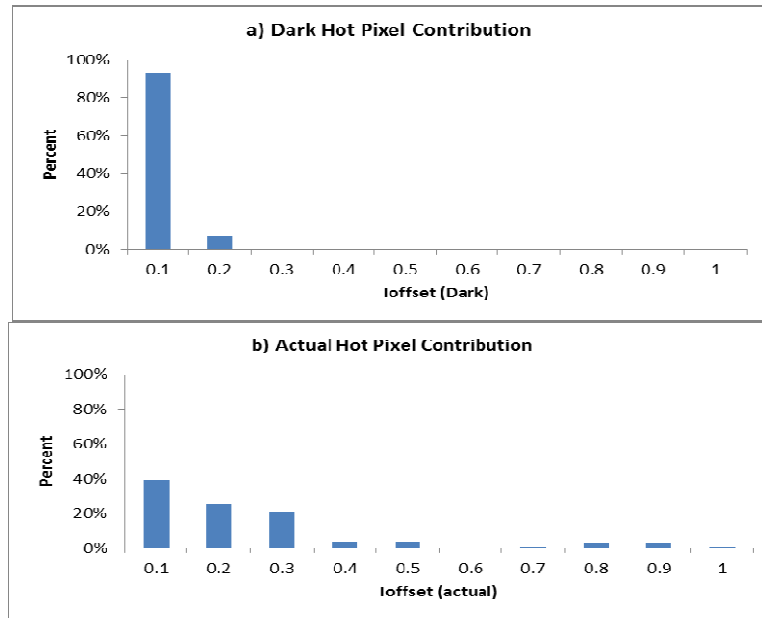


Figure 7: Hot pixel contribution for 1/125 sec exposure (a) calculated from dark hot parameters; (b) actual measured hot pixel contribution.

However, these results reveal an unexpected problem. In the 1/30 sec exposure (Figure 6), the dark hot pixel parameters give a good estimate of the error created by the defect, but in the 8x brighter 1/125 sec scene (Figure 7), the dark parameters (top histogram) show a much smaller defect contribution than the actual defect values.

After many experiments we came to the conclusion that the presence of sufficient light amplified the hot pixel parameters above and beyond the linear Equation (1). This effect is not discussed anywhere in the literature that we could find, and became an important modification that we made in our correction algorithm. It is further discussed in Section 7.



Figure 8: Higher complexity test image.

6. POSSIBLE LIMITATIONS IN DEFECT CORRECTION

The camera movement setup provides us a reliable and accurate method to obtain the real values of the defective pixels. Using this setup, we could compare the results of the three correction methods: interpolation ($A_m^{(i)}$), dark (D_m), and weighted (C_m) to the real pixel values. We first used as a test image the picture in Figure 3, and then repeated the experiment using the more complex image shown in Figure 8. We took the pictures over exposure times ranging from 1/125 sec to 1/60 sec, at a fixed ISO (800). We used this second image because the first test image had a bias toward

interpolation while this image has many more edges. Furthermore, the light intensity (R) in Figure 8 ranges from 0.0226 to 56.24 depending on the exposure time.

This last image (Figure 8) gave us an actual distribution of the hot pixel contribution (I_{offset}) (see Figure 9), where the contribution values are well above the noise floor (≤ 0.005). By examining Figure 9 we see that even the first bin is well above the noise floor, which makes this analysis statistically significant.

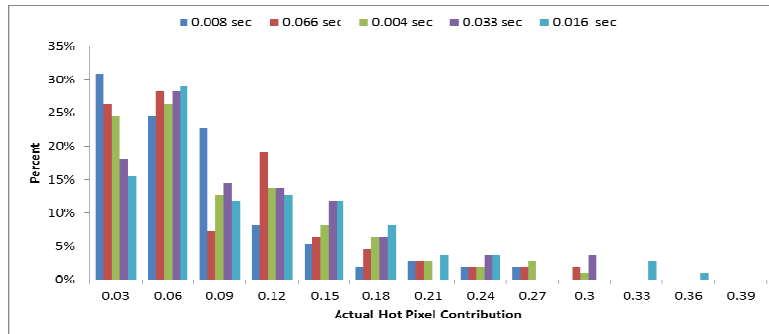


Figure 9: Distribution of Actual Hot Pixel Contribution.

Performing the interpolation correction method on the defective pixels to calculate $A_m^{(4)}$, we obtained the error distribution of $A_m^{(4)}$ shown in Figure 10. This error was calculated as the absolute value of $A_m^{(4)}$ minus the real pixel value. Examining the figure shows us that the interpolation correction method was effective, since most of the pixels are in the first four bins that represent errors below the noise floor (0.008).

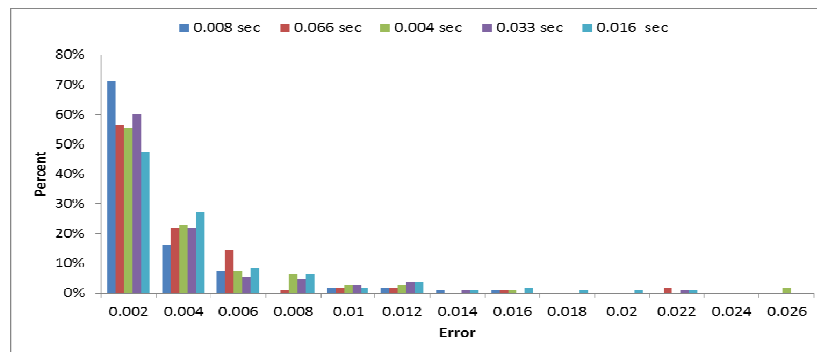


Figure 10: Error distribution of $A_m^{(4)}$

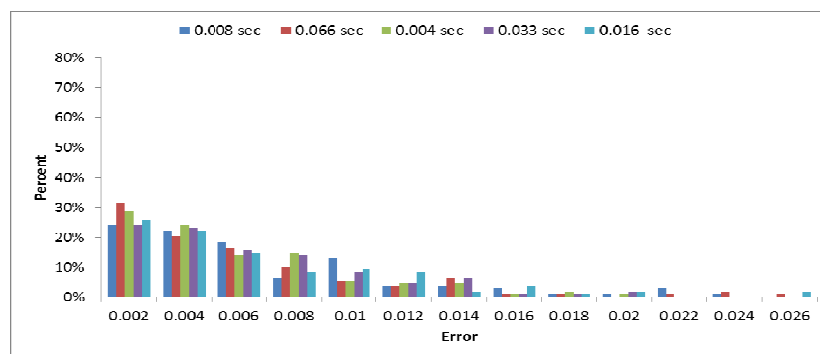


Figure 11: Error distribution of D_m .

By performing the dark correction method on the defective pixels to calculate D_m , we obtained the error distribution shown in Figure 11. Again, the error was calculated as the absolute value of D_m minus the real pixel value. Examining the figure shows us that the dark correction method was effective since most of the pixels are in the first four bins, but not as effective as the interpolation correction method.

For both methods, there are still a significant number of pixels (25%) that have a correction error outside of the noise floor while 75% are within the noise floor. To further compare the two corrections, we created in Figure 12 the distribution of the difference between the D_m error and the $A_m^{(4)}$ error.

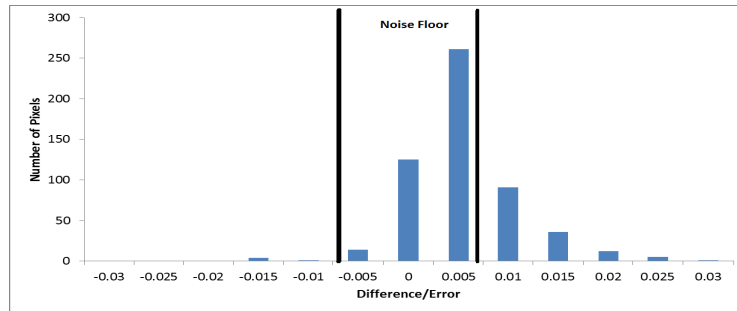


Figure 12: Distribution of D_m error minus $A_m^{(4)}$ error.

A negative difference means that the dark correction method is more accurate for the pixel, while a positive difference means that interpolation is better for this pixel. The distribution is centered at 0.005, indicating that the interpolation correction method is in general more effective. The majority of the pixels are still within ± 0.005 (below the noise floor of ± 0.008).

Performing the weighted correction method on the defective pixels to calculate C_m , we obtain the error distribution shown in Figure 13. Again, this error distribution was obtained by comparing C_m and the true pixel value. When calculating the weighted correction method, we determined the optimized correction weights ($\alpha = 0.918$, $\beta = 0.548$ and $\epsilon = 0.005$) by minimizing the total absolute error between C_m and the real pixel value using the Excel Solver.

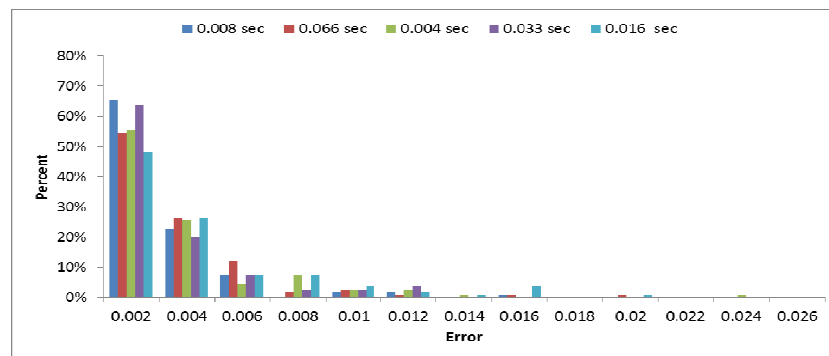


Figure 13: Error distribution of C_m .

This distribution shows that the weighted correction method is better than any of the two individual methods. A majority of the pixels now have an error below 0.005, and the number of pixels that have a higher error is statistically insignificant. This is due to the fact that the weighted algorithm takes advantage of both correction methods.

7. EFFECT OF ILLUMINATION ON HOT PIXEL BEHAVIOR

With the ability to extract the exact pixel data using the movement method, our data allowed us to extract the actual hot pixel value at any defect in the complex image of section 6. These results showed a strong indication that the hot pixels were, under some conditions, interacting with the illumination to change the hot pixel effect. In this section we discuss

the hot pixel behavior in the presence of various illumination levels. Traditionally, hot pixel concepts are studied using dark frame analysis. To further advance pixel correction, an understanding of how the defects behave in the presence of illumination is vital.

Equation (1) displays the classic hot pixel model. As mentioned previously, there is a dark component and a light illumination component. The light field component is proportional to the amount of incident light on the pixel. To extract the hot pixel behavior under illumination, we performed an experiment with our test camera by taking images of a uniformly illuminated scene at varying exposure times (1 sec to 0.00025 sec) and a range of illuminations. We set the exposure time and F#s to give us a constant $R_{photo}T$ value for a range of values from a very dark scene to a bright one. Since the image was very uniform, we extracted the illumination level (photocurrent R) for each pixel via local interpolation. Tests showed us that the pixel appeared to be sensitive not to the RT product (which determines the exposure level) but rather to the R (photocurrent) which is the illumination intensity hitting the pixel. Using Equation (8) to get the best curve fit, we were able to extract the a (offset) and b (dark current) parameters for pixels with a fixed illumination (R) value. We then performed a similar calculation for several defective pixels. We obtained the expected hot pixel data, and then generated the slope and offset of the hot pixel response under the influence of light. This was done for each F#, which is directly related to the illumination R at the pixel. Figures 14 and 15 show the slope and offset for a set of strong hot pixels, and we can see that both the slope and offset are not constant over the illumination R .

$$Y = a + bT + X \tag{8}$$

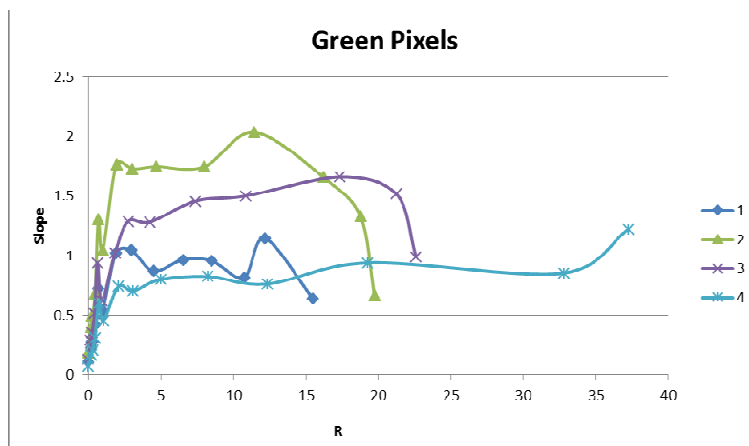


Figure 14: Hot pixel interaction with light illumination: Slope b vs R (illumination).

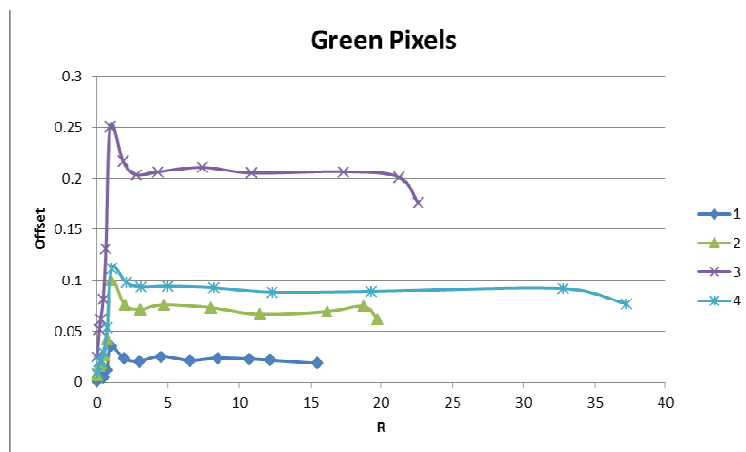


Figure 15: Hot pixel interaction with light illumination: Offset vs R (illumination)

Inspecting the above figures, we can see a general trend in the slope and offset responses. We can divide the response into 3 different regions. The first region shows a very drastic initial ramp to a maximum value. From initial analysis we

have observed that hot pixels with R lower than 2, and pixel values (including the hot pixel addition) smaller than 0.2, exhibit this behavior for both the slope and offset. In this region, the slope and offset responses are being enhanced and grow rapidly with the interaction to light. After an overshoot, we see the second region in which the slope and offset response is nearly constant. We found that the majority of pixel values of the hot pixels at these illuminations of between 0.2 and 0.8 display this behavior, where the enhancement seen in the previous region is declined. Lastly, at larger combined pixel values we see that the response breaks down. This is where the defective pixels values are near or at saturation.

It is clear that the usual behavior assumptions made for dark hot pixels are not valid in the illumination case. Additionally, this suggests that possibly the classic model described in Equation (1) is insufficient and inaccurate. Therefore, a further study of hot pixel behavior under the influence of light is needed in order to derive a more accurate model that will improve image correction. In our future research we will focus on characterizing pixel interaction with light and will develop a model to quantify this response.

8. CONCLUSIONS

This paper has described several methods of correcting hot pixel defects in images, and pointed out the problem in using the dark field characteristics of the hot pixel for correction. Using real images, we showed that although for modest illumination the hot pixel behaves closely to the dark field characteristics, at higher illuminations the light interacts with the damage to enhance the hot pixel effect. In our future research we will construct a more accurate model of the hot pixel response to illumination, which we will then use to develop improved correction algorithms that will combine this response with the surrounding pixel information.

REFERENCES

- [1] J. Dudas, L.M. Wu, C. Jung, G.H. Chapman, Z. Koren, and I. Koren, "Identification of in-field defect development in digital image sensors," *Proc. Electronic Imaging, Digital Photography III*, v6502, 65020Y1-0Y12, San Jose, Jan. 2007.
- [2] J. Leung, G.H. Chapman, I. Koren, and Z. Koren, "Statistical Identification and Analysis of Defect Development in Digital Imagers," *Proc. SPIE Electronic Imaging, Digital Photography V*, v7250, 742903-1 – 03-12, San Jose, Jan. 2009.
- [3] J. Leung, G. Chapman, I. Koren, and Z. Koren, "Automatic Detection of In-field Defect Growth in Image Sensors," *Proc. of the 2008 IEEE Intern. Symposium on Defect and Fault Tolerance in VLSI Systems*, 220-228, Boston, MA, Oct. 2008.
- [4] J. Leung, G. H. Chapman, I. Koren, Z. Koren, "Tradeoffs in imager design with respect to pixel defect rates," *Proc. of the 2010 Intern. Symposium on Defect and Fault Tolerance in VLSI*, 231-239, Kyoto, Japan, Oct. 2010.
- [5] J. Leung, J. Dudas, G. H. Chapman, I. Koren, Z. Koren, "Quantitative Analysis of In-Field Defects in Image Sensor Arrays," *Proc. of the 2007 Intern. Symposium on Defect and Fault Tolerance in VLSI*, 526-534, Rome, Italy, Sept. 2007.
- [6] J. Leung, G.H. Chapman, Y.H. Choi, R. Thomas, I. Koren, and Z. Koren, "Analyzing the impact of ISO on digital imager defects with an automatic defect trace algorithm," *Proc. Electronic Imaging, Sensors, Cameras, and Systems for Industrial/Scientific Applications XI*, v 7536, 75360F1-0F12, San Jose, Jan. 2010
- [7] A.J.P. Theuwissen, "Influence of terrestrial cosmic rays on the reliability of CCD image sensors. Part 1: experiments at room temperature," *IEEE Transactions on Electron Devices*, Vol. 54 (12), 3260-6, 2007.
- [8] A.J.P. Theuwissen, "Influence of terrestrial cosmic rays on the reliability of CCD image sensors. Part 2: experiments at elevated temperature," *IEEE Transactions on Electron Devices*, Vol. 55 (9), 2324-8, 2008.
- [9] G.H. Chapman, J. Leung, A. Namburete, I. Koren and Z. Koren, "Predicting pixel defect rates based on image sensor parameters," *Proc. IEEE Int. Symposium on Defect and Fault Tolerance*, 408-416, Vancouver, Canada, Oct. 2011.
- [10] G.H. Chapman, J. Leung, R. Thomas, I. Koren, and Z. Koren, "Projecting pixel defect rates based on pixel size, sensor area and ISO," *Proc. Electronic Imaging, Sensors, Cameras, and Systems for Industrial/Scientific Applications XII*, v8298, 82980E-1-E-11, San Francisco, Jan. 2012
- [11] D. Wan, P.Askey, S.Joinson, A. Westlake, R. Butler, "Canon EOS 5D Mark II In-depth Review," 2014. Available: <http://www.dpreview.com/reviews/canoneos5dmarkii/> 21